Appl. Phys. B 67, 667–673 (1998)

Applied Physics B
Lasers
and Optics

Thermal grating and broadband degenerate four-wave mixing spectroscopy of OH in high-pressure flames

H. Latzel[1], A. Dreizler[1,*], T. Dreier[1], J. Heinze[2], M. Dillmann[2], W. Stricker[2], G.M. Lloyd[3], P. Ewart[3]

[1] Physikalisch Chemisches Institut, Universität Heidelberg, Im Neuenheimer Feld 253, D-69120 Heidelberg, Germany
[2] DLR, Institut f. Physikalische Chemie der Verbrennung, Pfaffenwaldring 38-40, D-70569 Stuttgart, Germany
[3] Clarendon Laboratory, Oxford University, Parks Road, Oxford OX1 3PU, UK
(E-mail: p.ewart@physics.oxford.ac.uk)

Received: 10 November 1997/Revised version: 28 May 1998

Abstract. Time-resolved light scattering from thermal gratings induced by absorption of pulsed laser light resonant with transitions in the $A^2\sum$–$X^2\Pi(0,0)$ band of OH has been studied in premixed methane/air flames using a cw Ar^+ laser probe. Measurements of flame temperature and pressure were derived from fits of theoretical simulations to the observed time variation of signals over a pressure range of 10 to 40 bar and for different stoichiometry that were in agreement with independent measurements using N_2 CARS and predictions of a one-dimensional flame calculation. Broadband DFWM spectra in the same band of OH were observed up to a pressure of 9 bar, above which signals were obtained only from scattering from thermal gratings.

PACS: 42.62.Fi; 84.40.Py

Optical techniques for diagnostics of flames are attractive owing to their non-intrusive character and their ability to provide spatially and temporally resolved measurements of important parameters governing the combustion processes. Recently degenerate four wave mixing, DFWM, has received much attention as a diagnostic technique for combustion and plasma environments. Detection of trace species in flames [1] and plasmas [2], measurements of flame temperatures in one [3] and two [4] dimensions and velocimetry of non-combusting flows [5] have been achieved using DFWM. Multiplex, or broadband, DFWM [6] has been used to make single-shot temperature measurements in flames [7, 8].

The DFWM signal is produced by a non-linear optical process in which each one of two intense laser beams, the pumps, interferes with a third beam, the probe, to induce a spatially periodic modification of the molecular populations in a resonantly absorbing medium. This *population grating* results in a corresponding spatial modulation of the absorption or dispersion properties of the medium leading to scattering of the other pump beam to give a coherent, laser-like, signal beam. In many technical flames the combustion takes place at elevated pressures and so the effects of high pressures on DFWM signals is an important consideration [9, 10]. It has been shown that the use of saturating laser intensities may make the DFWM signals insensitive to collisional effects which, in the unsaturated case, lead to a dramatic reduction in signal levels [11]. However collision-induced relaxation effects may lead also to a rapid transfer of energy from the molecular excited states into thermal energy which will be also disposed in a grating-like pattern. This *thermal grating* will scatter light coherently into the phase matched signal direction and make a contribution to the measured signal. At high pressures, or in rapidly quenching media, this laser induced thermal grating scattering, LITGS, may dominate the DFWM signal from the population grating [12]. These thermal gratings have been used to measure gas dynamic properties [13, 14] and their relative contribution to DFWM signals has also been studied [15]. Such laser-induced transient gratings have been exploited for some time to study diffusion and other relaxation processes in condensed phases [16].

In general a four-wave mixing signal may have contributions from both population and thermal gratings. By use of crossed polarizations in the two pump beams the formation of the intensity grating, which relaxes to form the thermal grating, may be prevented [17, 18]. On the other hand, the thermal grating may be distinguished from the population grating by virtue of its dynamical behaviour [13]. A probe beam having a different wavelength may be used, as in the present work, to measure the time behavior of the LITGS signal.

We report experimental studies of LITGS and broadband DFWM in OH formed in a methane/air flame at pressures in the range 1 to 40 bar. The LITGS studies were carried out by generating the thermal grating using a pulsed, narrow-bandwidth, dye laser and probing it with a cw laser. Analysis of the time behaviour of the signals is shown to yield measurements of temperature and pressure or, alternatively, gas transport parameters. Broadband DFWM signals were generated using a pulsed and frequency-doubled broad-bandwidth laser. The signals were found to have contributions from scat-

* *Present address*: Universität Stuttgart, Institut für Technische Verbrennung, Pfaffenwaldring 12, D-70569, Stuttgart, Germany

tering off both population and thermal gratings and are shown to be dominated by LITGS signals at pressures above 9 bar.

1 Theoretical considerations

The signals from both thermal and population gratings are generated by Bragg scattering from the spatially periodic perturbations to the complex refractive index of the medium. The grating picture of DFWM consists of the signal being created by scattering of one pump beam off the population grating formed by interference between the other pump and the probe beam, with all beams having the same frequency. The LITGS process may be described by the generation of a thermal grating following interference of two pump beams, with the signal arising from scattering from this grating of a probe beam which may have a different frequency. Interference of two pump beams, of wavelength λ_1, intersecting at an angle, θ, establishes a grating of spacing, Λ, given by

$$\Lambda = \lambda_1/(2\sin\theta/2)\ .$$

Absorption of light followed by rapid, collisionally induced quenching leads to a corresponding spatially periodic energy deposition in the medium. The resulting perturbation in temperature and pressure leads to a perturbation of the medium density, the evolution of which has been treated by solving one-dimensional, linearized hydrodynamic equations [12, 14]. A nearly static pattern of temperature perturbation is produced which decays by thermal diffusion. A simultaneous pressure variation or standing wave pattern is also imposed on the medium, which corresponds to two counter-propagating acoustic waves which decay by viscous damping. As the acoustic waves travel across the thermal grating the total scattering efficiency is modulated in time with a period determined by the local sound speed in the medium, c_o. Both thermal and acoustic contributions decay at rates determined by the dynamic properties of the gas. Our experimental results have been analysed using the model of Paul et al. [12] although an additional correction was found necessary to account for the decay of the acoustic waves as they escape a small interaction volume as described by Cummings et al. [14]. The scattering efficiency of the gratings, and hence the LITGS signal intensity, is proportional to the square of the density perturbation ρ', which is found to be [12]:

$$\rho' = -(2\pi)^2 \frac{\gamma-1}{\gamma}\frac{\alpha}{P_o}\frac{8E_p}{\pi d^2}\cos(2\pi\xi)\,Z(\zeta)\ ,$$

where γ is the ratio of specific heats, c_p/c_v, E_p is the total flux in each of the interfering pump beams, of spot size d, and P_o is the equilibrium pressure. α is the total absorption coefficient determined by the Einstein B coefficient and the absorbing-state population density. The cosine term represents the spatially periodic modulation in terms of a normalized length parameter $\xi = x/\Lambda$ and $Z(\zeta)$ is a similarly non-dimensional function describing the temporal oscillations and decay of the density perturbation where $\zeta = c_o t/\Lambda$. The decay rate and oscillation period of $Z(\zeta)$ is determined by the Prandtl, Schmidt, and Reynolds numbers characterizing the medium and the model is applied in the limit of large Reynolds numbers, $\mathrm{Re} \gg 1$, which corresponds to the condition that the grating spacing is much larger than the mean free path in the gas. The Schmidt number is also assumed to be large, i.e. molecular diffusion is slow on the time scale of the LITGS signal build-up and decay.

Theoretical treatments of DFWM induced by broadband lasers have been presented previously dealing with the signal intensity [19], time behavior [20], and spectral lineshape [21]. In some cases temperatures have been derived from the multiplex spectral intensities using a dependence on line strength and population density equivalent to that for monochromatic excitation [7, 8]. Owing to experimental factors the data obtained in this work was insufficiently reliable to allow accurate temperatures to be derived from the broad-bandwidth DFWM spectra.

2 Experimental apparatus and procedure

Signals from both broadband DFWM and LITGS were generated from OH produced in a methane/air flame in the DLR high-pressure burner described in detail elsewhere [22]. Optical access was afforded to the flame along two orthogonal axes. LITGS and DFWM signals were generated by lasers propagating along one axis and simultaneous laser-induced fluorescence, LIF, signals were observed along the other axis. Measurements were made 1.5 mm above the 8-mm-diameter, porous brass plate of the burner. The temperature at the measurement point was well characterized by previous measurements using coherent anti-Stokes Raman Scattering, CARS, and spontaneous Raman scattering from N_2 [23].

The experimental arrangement used to study the LITGS signals is shown in Fig. 1. The pump beams were provided by the frequency-doubled output of a narrow-bandwidth pulsed dye laser (Lumonics HD500) excited by a frequency-doubled Nd:YAG laser (Spectra Physics). The thermal grating was produced by focusing the pump beams using a 1000-mm focal length lens, crossing them at an angle of 2.4° and tuning the wavelength, λ_1, to transitions in the $A^2\sum$–$X^2\Pi(0,0)$ band of OH around 307 nm. An energy of up to a maximum of 1.7 mJ in each pump beam was used to achieve reasonable signal-to-noise levels when pumping the $R_1(5)$ line. The probe beam at wavelength λ_2 was arranged to be at an angle

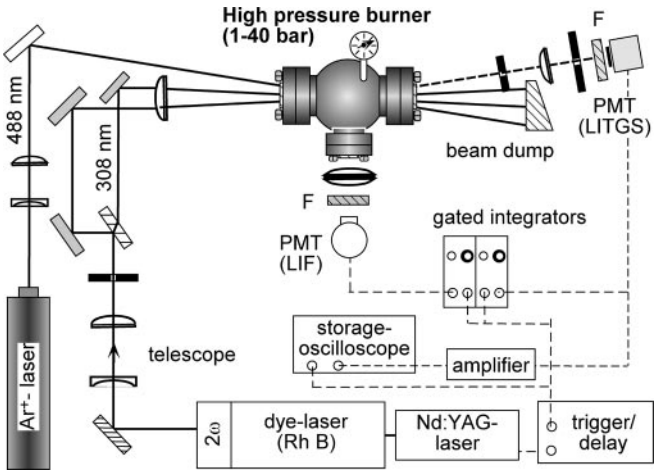

Fig. 1. Experimental setup for time-resolved LITGS from OH in a high-pressure flame. F denotes an interference filter

φ with respect to the bisector of the crossed pump beams satisfying the Bragg condition:

$$2 \sin \varphi = \lambda_2 / \Lambda \ .$$

The cw output of an argon ion laser ($\lambda_2 = 488$ nm), having a power of 1.25 W and directed at an angle $\varphi = 1.9°$, was used to probe the thermal grating. The reflected signal was passed through a set of pin-holes to reject stray light and detected with a photomultiplier. To study the time behaviour of the LITGS signal the photomultiplier output was measured with a fast digital storage oscilloscope (sample rate 2 GHz). The spectral response was recorded by tuning the pump laser across the $A^2\sum$–$X^2\Pi(0, 0)$ band and detecting the signal intensity using a boxcar averager (Stanford Research SRS 250). LIF signals were also recorded simultaneously with the scanning of the pump laser. Both temporal and spectral data was stored and processed on a laboratory computer.

Broadband, or multiplex, DFWM spectra of the $A^2\sum$–$X^2\Pi(0, 0)$ band of OH were recorded using the experimental arrangement shown in Fig. 2. A broadband, modeless, laser [24], spectrally tuned by an interference filter and containing two amplifier stages (Mode-x Laser Systems, ML-3) was pumped by a frequency-doubled Nd:YAG laser and the output frequency-doubled using two KD*P crystals in tandem. The demands of critical phase matching restricted the bandwidth that could be frequency-doubled in one crystal to about 10 cm^{-1}. The use of two crystals allowed two independently tunable spectral regions of the dye laser spectrum to be frequency-doubled and thus a larger number of transitions could be excited. The forward-folded BOXCARS phase-matching arrangement [25] was used to generate the DFWM signals. This geometry offers better signal-to-noise levels than the commonly used counter-propagating, or phase-conjugating arrangement, since no beam splitters are needed to pick out the signal beam from the much stronger probe beam. Furthermore, the forward geometry is found to be less sensitive to beam steering effects arising from high refractive index gradients in some combustion applications. The phase-conjugating geometry offers improved spectral resolution when narrowband lasers are used owing to the selection of one velocity sub-group from the Doppler-broadened spectrum. However this advantage is lost when using broadband excitation and so the forward geometry is most suitable in this case. Four parallel beams were produced from the frequency-doubled dye laser output using two specially fabricated quartz blocks having suitable dielectric coatings on input and exit faces. The beams were focused by a 500-mm focal length lens to cross at an angle of 1.6° in the measurement region of the flame. Three of the beams, two pumps and a probe, were used for signal generation. The fourth is used to trace the signal beam path for alignment and is blocked during the experiment. The signal beam is passed through an aperture, blocking the pump and probe beams, and is directed through a single-stage grating spectrograph (1.3 m focal length, 2400 l/mm holographic grating) equipped with a rear-illuminated CCD camera (Princeton Instruments). The overall spectral resolution of the system was 0.2 cm^{-1}. Part of the excitation beam energy was directed to the spectrometer via an optical fiber to fall on a different part of the CCD chip to allow simultaneous recording of the laser spectrum.

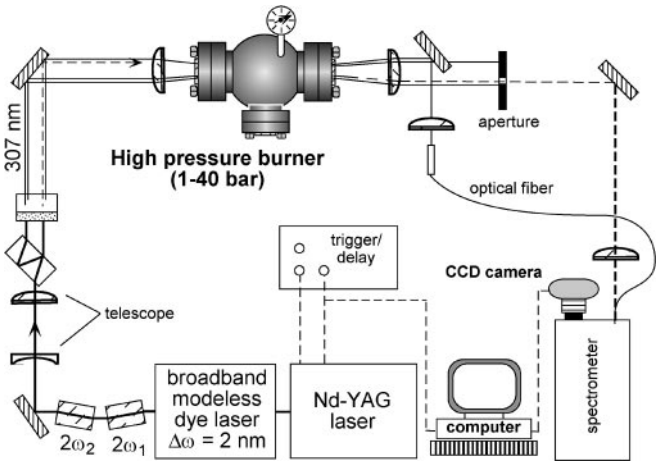

Fig. 2. Experimental setup for broadband, multiplex, DFWM of OH in a high-pressure flame. $2\omega_1$ and $2\omega_2$ denote KD*P crystals used to generate, by frequency-doubling different parts of the broadband output of the modeless laser, a beam containing two independently tunable bands of UV light around 307 nm. After the telescope the UV beam is divided into four parallel beams by the two specially coated quartz blocks. A fraction of one UV beam emerging from the burner is coupled into an optical fibre and delivered to the spectrograph to record the laser spectrum simultaneously with the broadband DFWM signal

3 Results and analysis

The temporal behaviour of the LITGS signals was recorded at different values of pressure and stoichiometry. All the time-resolved data presented here are results of single-shot recordings following excitation of the $R_1(5)$ line. Figure 3 shows the time behaviour of the LITGS signal in a stoichiometric flame at pressures of 10, 20, and 40 bar. The oscillation arising from the acoustic wave and the decay by viscous damping and thermal dissipation is clearly shown by the data. Furthermore, the decrease in decay rate with increasing pressure is evident.

Theoretical simulation of this data was based on the theoretical model of Paul et al. [12]. In our analysis the thermal grating was assumed to be established rapidly during the excitation pump pulse, i.e. the quenching is taken to be

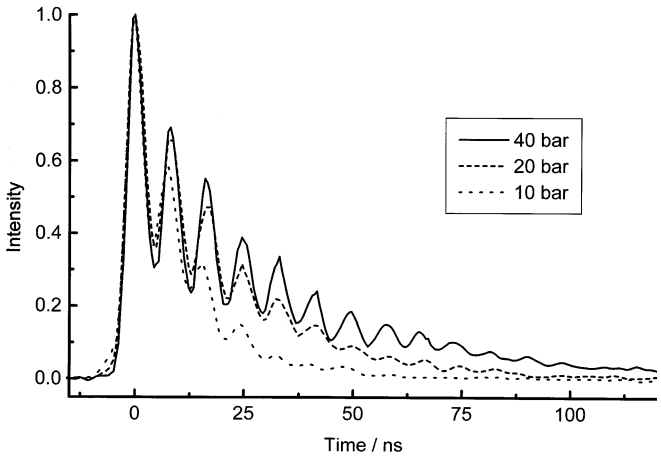

Fig. 3. Time-resolved LITGS signals recorded from the flame at pressures of 10, 20, and 40 bar. Note the reduction in decay rate as the pressure is increased

sufficiently fast so that the build-up time of the thermal grating may be ignored on the time scale of the pump pulse and subsequent grating decay. This assumption is validated by measurements of the quenching rate, $Q \simeq 0.5\,\mathrm{ns}^{-1}$, for a typical excited state of OH in a flame at atmospheric pressure [26]. At higher pressures the quenching rate is assumed to be $Q = 0.5 \times P\,\mathrm{ns}^{-1}$, where P is the pressure in units of bars. The absorption line-strength data were determined using published values of Einstein A-coefficients for OH [27]. The dynamics of the thermal grating decay are determined by the gas transport properties and hence on the species present. The local composition of the gas in the measurement volume was estimated from one-dimensional flame-code calculations [28] and previous exhaust gas measurements. Values of thermodynamic properties; density, heat capacity (c_p, c_v), viscosity, μ, and thermal conductivity, K, of the gas mixture, were obtained from, or calculated using, published data [29].

Figure 4 shows a typical LITGS signal as a function of time for a 40-bar flame, stoichiometry $\phi = 1$, together with a best-fit simulated signal calculated numerically using temperature, T, and pressure, P, as the fitting parameters. The quality of fit was improved by allowing input parameters to vary within a range of uncertainty reflecting experimental errors in laser pulse width, detector response time and the thermal grating spacing. Although the grating spacing, Λ, was determined by geometrical measurements of the pump beam crossing angle, to be 7.3 μm, a residual uncertainty arose from inaccuracy in determining the crossing angle and possible deviations of the beams in traversing strong refractive index gradients in the flame. A variation of 5.5% in Λ allowed a better fit to the data and a derived temperature in better agreement with independent measurements using N_2 CARS. We note that other work on thermal gratings in atmospheric-pressure flames encountered similar uncertainty in determining the grating spacing. Errors of between 15% and 20% were quoted [30]. The determination of the grating spacing is the source of largest single error in the present work and the resulting systematic error limits the confidence in the accuracy of the derived absolute temperature. The mean value of 10 separate measurements yielded a temperature of 2101 K with a standard deviation of 85 K in good agreement with CARS measurements of 2015 ± 60 K under similar flame conditions.

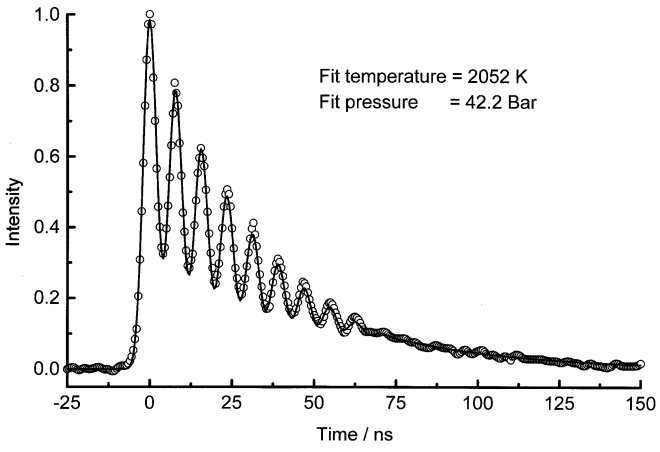

Fig. 4. Time-resolved LITGS signal from methane air flame at 40 bar, $\phi = 1$. *Open circles* denote experimental (single-shot) data and the *solid line* is a best fit theoretical simulation adjusted for temperature and pressure

Owing to conduction of heat to the burner plate the flame temperature is lower than the calculated adiabatic temperature of 2320 K at 40 bar. The pressure derived from such fits had a mean value of 43 ± 2.6 bar in reasonable agreement with the static pressure transducer value of 40 bar. Similar quality of fit of simulated to experimental data was obtained for stoichiometric flames at 20 bar.

Temperatures and pressures were also derived from signals obtained in flames of different stoichiometry at 40 bar. Values are listed in Table 1, which lists the mean values of T and P derived from N data sets. It is seen that the temperatures were found to be lower for the richer flames ($\phi > 1$) in accord with predictions of the adiabatic flame model calculations. The apparent slight improvement in precision with increasing equivalence ratio is not statistically significant owing to the small data base. The errors in the pressure measurements are significantly larger than those for the temperature since fitting the decay curve is more affected by noise than the fit to the oscillations which determine the temperature, especially as the signal tails off at longer times.

The temperature at 10 bar was measured to be 2186 ± 54 K which is higher than that at higher pressures owing to reduced heat loss as the flame sits further away from the burner surface. However this value is still lower than the calculated adiabatic flame temperature, $T_\mathrm{ad} > 2300$ K at 10 bar.

The simulation of data obtained at 10 bar was noticeably less good as shown in Fig. 5, from which the temperature of 2186 ± 54 K and a pressure of 14.2 ± 0.5 bar were derived. The main reason for the relatively poor fit is the breakdown of

Table 1. Mean values of T and P from N data sets

Pressure /bar	ϕ	Fitted temp. /K	s.d. temp. /K	Fitted press. /bar	s.d. press. /bar	N
40	1.0	2101	85	43	2.6	10
40	1.2	2068	50	41.2	3.6	10
40	1.6	1920	43	31.9	4.5	5
20	1.0	2139	46	24.4	2.2	5

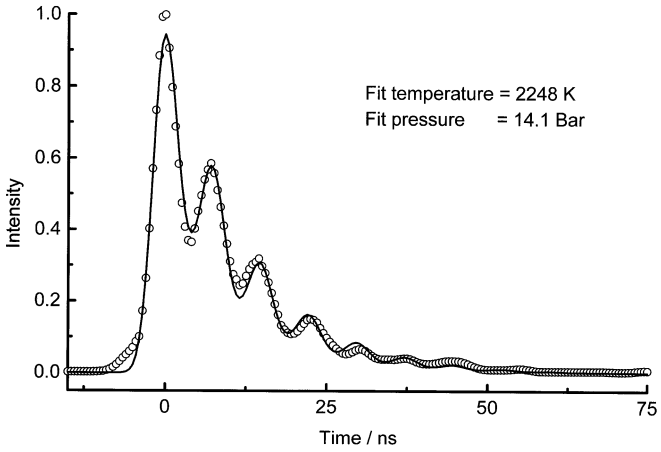

Fig. 5. Time-resolved LITGS signal from methane air flame at 10 bar, $\phi = 1$. *Open circles* denote experimental (single-shot) data and the *solid line* is a best fit theoretical simulation adjusted for temperature and pressure. The simulation does not properly account for the different rates of relaxation leading to the thermal grating at this pressure, the time scales of which are significant relative to the overall signal lifetime

the assumptions of the model. At the lower pressure the decay of the LITGS signal is no longer slow on the time scale of the grating formation and laser pulse duration. Thus the initial stage of the signal is affected by thermal and acoustic signals generated with a continuously shifting phase. Furthermore the assumption of rapid transfer of excitation energy to the thermal grating may no longer be valid. A two-step relaxation mechanism with two differing relaxation rates governing the internal (vibration–rotation) to translational energy transfer will distort the initial decay of the signal [12]. A lack of knowledge of these relaxation rates precludes accurate modelling of this mechanism. A similar two-step relaxation process was noted in the generation of thermal gratings via absorption by OH in an H_2/O_2 flame at atmospheric pressure where the effect is even more significant [30]. The systematic error resulting from these uncertainties leads to an upward shift in derived temperatures. When the fitting is weighted towards the final stages of the decay a lower temperature is obtained.

The data has been analysed, using calculated values of gas transport properties, to derive values of temperature and pressure so that the results could be compared with independent measurements of these parameters. In principle the values of T and P could be taken from these other measurements and the data used to derive values of the gas transport properties [31–33]. Over the entire pressure range studied the signals were seen to be dominated by LITGS with no significant contribution from scattering from electrostrictive gratings [13, 34].

LITGS has been shown to yield spectra of pure gases such as O_2 and CO_2 in cells by absorption [35] or Raman pumping [36]. In the present work LITGS spectra of the radical flame species, OH, were produced by scanning the wavelength, λ_1, of the pump lasers and monitoring the scattered signal from the Ar^+ ion laser probe beam. Provided λ_1 does not vary over too large a range, the grating spacing does not change significantly and the probe beam, incident at angle φ, will continue to be scattered efficiently. The LITGS signal thus gives a measure of the absorption spectrum of the molecule as λ_1 is scanned. Such a LITGS spectrum is shown in Fig. 6 for part of the R-branch in a 10-bar flame. A simultaneously recorded LIF signal is also shown for comparison.

The LITGS spectra obtained in the present work, exhibit a higher resolution and a higher signal-to-noise, S/N, ratio than the corresponding LIF spectrum under these conditions. The higher resolution results from the nonlinear nature of the LITGS process – the signal lineshape depends quadratically on the absorption rather than linearly as in LIF. The improved S/N ratio arises from the coherent nature of the LITGS signal which is emitted as a laser-like beam allowing more effective discrimination against background light and laser scatter from the flame than is possible with the incoherent LIF signal. A further advantageous feature of the LITGS signal is its quadratic dependence on the species concentration. As the pressure increases the quenching becomes more effective in producing the thermal grating whereas the increasing quenching leads to a reduction in the LIF signal. In principle the LITGS spectrum could be analysed to yield temperatures from the relative intensities of lines from rotational energy levels in Boltzmann equilibrium. The data recorded in the present work used strongly saturating pump

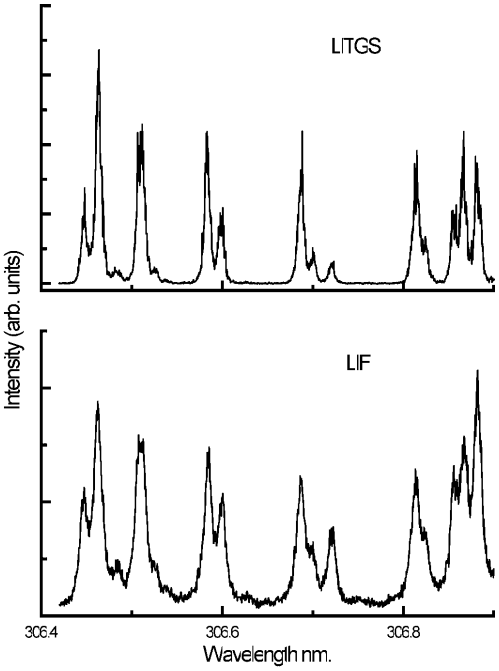

Fig. 6. Simultaneously recorded LITGS and LIF spectra from methane/air flame at 10 bar pressure showing part of the $A^2\sum\text{–}X^2\Pi(0,0)$ band of OH

beams, which leads to significant contributions from absorption in satellite features in the OH spectrum. A quantitative theory to account for the saturation behaviour of the LITGS signals and the complex relaxation processes leading to the thermal grating formation is not at present available. A preliminary attempt to simulate the LITGS spectrum was made using the model of Paul et al. [12]. Fits to the measured spectrum yielded temperatures that were systematically lower than values measured by CARS or using the time-resolved decay of the LITGS signal indicating the need for a detailed theory of spectral intensities arising from LITGS.

Broadband DFWM spectra of OH were recorded from stoichiometric flames in the pressure range 1 to 30 bar. The bandwidth of the laser spectrum was adjusted to provide two independently tunable regions which covered parts of the R_1 and R_2 branches of the $A^2\sum\text{–}X^2\Pi(0,0)$ band. Single-shot spectra were obtainable up to pressures of about 3 bar. At higher pressures the signal levels fell as a result of collisional effects so that averaged spectra of an increasing number of single shots were required to achieve signals above the camera noise level. Figure 7 shows broadband DFWM spectra recorded at increasing pressure. At 1 bar up to eight transitions in the $A^2\sum\text{–}X^2\Pi(0,0)$ band are resolved and resonant structure is apparent up to 9 bar. Above about 6 bar this structure appeared superimposed on a broad spectral background. At higher pressures only the broad spectral feature approximately following the shape of the incident laser spectrum was observed. This broad spectral signal is attributed to LITGS since it displayed all the features of a four-wave mixing signal. The thermal grating is formed by resonant absorption at the molecular transition wavelengths overlapped by the laser spectrum. The spread in excitation wavelengths, λ_1, and probe wavelengths, λ_2, contained in the incident broadband laser is such that the angular divergence of Bragg-scattered

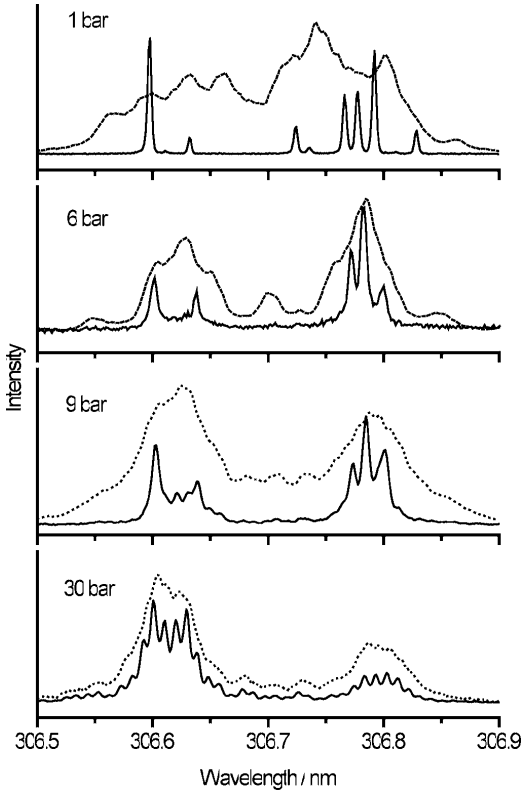

Fig. 7. Broadband, multiplex, DFWM spectra (*solid line*) recorded in the methane/air flame at different pressures together with simultaneously recorded laser spectra (*dashed line*). 1-bar spectrum: single shot; 6-bar spectrum: average of 5 shots; 9-bar spectrum: average of 10 shots; 30-bar spectrum: average of 50 shots

signals from different gratings formed over this range is less than the laser beam divergence. Thus LITGS signals could be collected effectively over the whole bandwidth of the incident laser. Owing to instabilities in the intensity and spatial beam profile of the Nd:YAG pumping laser and consequently in the broadband UV output, fluctuations in the spectral intensity of the DFWM spectra precluded reliable derivation of temperature from the data. However these results indicate that thermometry using broadband DFWM of OH could, in principle, be feasible up to 6 bar, and possibly up to a maximum of 9 bar, for methane/air flames. Above this pressure only scattering from thermal gratings was measurable. In the intermediate regime the signals contain significant contributions from both population and thermal gratings. One potential advantage of using broadband DFWM is that the relative contribution of the LITGS signal is apparent from the intensity of the broad background signal on which the resonant DFWM signal is superimposed.

4 Conclusions

LITGS signals from OH in methane/air flames have been recorded in flames of different stoichiometry and over a pressure range of 10 to 40 bar. Broadband DFWM spectra of OH have been recorded in the same flame at pressures from 1 to 30 bar. Results indicate that broadband DFWM of OH should be feasible for thermometry up to 6 bar. Analysis, using the model of Paul et al. [12] showed that temperature and pressure values can be deduced from the temporal behaviour of the LITGS signals in high-pressure flames. Accurate results were obtained from the data for flames at 20–40 bar. Data from flames at pressures of 10 bar or lower, will need a more detailed model of the thermal grating dynamics to take account of multiple-stage relaxation mechanisms and the finite duration of the incident laser pulses and detector response times. These results indicate that LITGS is a viable method for measurement of temperature and pressure in high-pressure flames. Alternatively, if P and T are known from other measurements the LITGS signals may yield measurement of other gas dynamic properties that would be difficult to determine by other means in high-pressure combustion. Since measurements based on LITGS decay do not depend on absolute or relative signal magnitudes, but only on time or frequency data they are insensitive to fluctuations in laser intensity. LITGS signals provide a time- and space-resolved absorption measurement which is sensitive to minor species and may thus provide an alternative to LIF in high-pressure combustion studies. In practice the spatial resolution can only be increased at the cost of impairing the time resolution, since the acoustic wave components of the induced grating will escape the measurement volume more quickly as this is reduced. Accuracy and precision of measurements will be limited by uncertainties in determination of the induced grating spacing and knowledge of the local gas composition.

Acknowledgements. The authors are grateful to the British Council and the D.A.A.D. for financial support of this work. The work on the high pressure burner at DLR was partially supported by the B.M.B.F. under contract No. 13N6119 and this is gratefully acknowledged. GML is grateful to the Engineering and Physical Sciences Research Council (U.K.) and Shell Research Ltd for personal financial support. PE is grateful to BG plc and the Royal Academy of Engineering (U.K.) for support.

References

1. P. Ewart, S.V. O'Leary: Opt. Lett. **11**, 279 (1986)
2. T.G. Owano, C.H. Kruger, D.S. Green, S. Williams, R.N. Zare: Diamond and Relat. Mater. **2**, 661 (1993)
3. T. Dreier, D.J. Rakestraw: Opt. Lett. **15**, 72 (1990)
4. P. Ewart, M. Kaczmarek: Appl. Opt. **30**, 3996 (1991)
5. R.B. Williams, P. Ewart, A. Dreizler: Opt. Lett. **19**, 1486 (1994)
6. P. Ewart, P. Snowdon: Opt. Lett. **15**, 1403 (1990)
7. B. Yip, P.M. Danehy, R.K. Hanson: Opt. Lett. **17**, 751 (1992)
8. I.P. Jefferies, A.J. Yates, P. Ewart: In *Coherent Raman Spectroscopy – Applications and New Developments*, ed. by E. Castellucci, R. Righini, P. Foggi (World Scientific, Singapore 1992) p. 129
9. D.A. Feikema, E. Domingues, M-J. Cottereau: Appl. Phys. B **55**, 424 (1992)
10. H. Bervas, B. Attal-Tretout, S. Le Boiteux, J-P Taran: J. Phys. B: At. Mol. Opt. Phys. **25**, 949 (1992)
11. P.M. Danehy, E.J. Friedman-Hill, R.P. Lucht, R.L. Farrow: Appl. Phys. B **57**, 243 (1993)
12. P.H. Paul, R.L. Farrow, P.M. Danehy: J. Opt. Soc. Am. B **12**, 384 (1995)
13. E.B. Cummings: Opt. Lett. **19**, 1361 (1994)
14. E.B. Cummings, I.A. Leyva, H.G. Hornung: Appl. Opt. **34**, 3290 (1995)
15. P.M. Danehy, P.H. Paul, R.L. Farrow: J. Opt. Soc. Am. B **12**, 1564 (1995)
16. H.J. Eichler, P. Günter, D.W. Pohl: *Laser-induced Dynamic Gratings*, Springer Series in Opt. Sci. (Springer, Berlin, Heidelberg 1986)
17. S. Williams, R.N. Zare, L. Rahn: J. Chem. Phys. **101**, 1072 (1994)
18. J.F. Lam, R.L. Abrams: Phys. Rev. A **26**, 1539 (1982)
19. J. Cooper, A. Charlton, D. Meacher, P. Ewart, G. Alber: Phys. Rev. A **40**, 5705 (1989)

20. M. Kaczmarek, D. Meacher, P. Ewart: J. Mod. Opt. **37**, 1561 (1990)
21. P.G.R. Smith, P. Ewart: Phys. Rev. A **54**, 2347 (1996)
22. H. Eberius, T. Just, T. Kick, G. Häfner, W. Lutz: Proc. Joint Meeting German/Italian Sections Comb. Institute, Ravello (1989) p. 3
23. M. Woyde, W. Stricker: Appl. Phys. B **50**, 519 (1990)
24. P. Ewart: Opt. Commun. **55**, 124 (1985)
25. A.C. Eckbreth: Appl. Phys. Lett. **32**, 421 (1978)
26. T.A. Reichardt, M.S. Klassen, G.B. King, N.M. Laurendeau: Appl. Opt. **35**, 2125 (1996)
27. A. Goldman, J.R. Gillis: J. Quant. Spectrosc. Radiat. Transfer **25**, 111 (1980)
28. J. Warnatz: 18th Int. Combustion Symposium, The Combustion Institute, 369 (1981)
29. R.C. Reid, J.M. Prausnitz, B.E. Poling: *The Properties of Gases and Liquids*, 4th edn. (McGraw-Hill, New York 1987)
30. S. Williams, L.A. Rahn, P.H. Paul, J.W. Forsman, R.N. Zare: Opt. Lett. **19**, 1681 (1994)
31. M. Terazima, N. Hirota: J. Chem. Phys. **95**, 6490 (1991)
32. Y. Kimura, D. Kanda, M. Terazima, N. Hirota: Ber. Bunsen-Ges. Phys. Chem. **99**, 196 (1995)
33. E.B. Cummings, H.G. Hornung, M.S. Brown, P.A. DeBarber: Opt. Lett. **20**, 1577 (1995)
34. B. Hemmerling, A. Stampanoni-Panariello: Appl. Phys. B **57**, 655 (1995)
35. B. Hemmerling, R. Bombach, W. Hubschmidt: Chem. Phys. Lett. **256**, 71 (1996)
36. D.N. Kozlov, R. Bombach, B. Hemmerling, W. Hubschmidt: Opt. Lett. **22**, 46 (1997)